Heliyon 8 (2022) e10216

Contents lists available at ScienceDirect

Heliyon

journal homepage: www.cell.com/heliyon

Research article

The detection of multiple analytes by using visual colorimetric and fluorometric multimodal chemosensor based on the azo dye

Hong Ren **, Fei Li, Shihua Yu, Ping Wu *

School of Chemistry and Pharmaceutical Engineering, Jilin Institute of Chemical Technology, Jilin City, 132022, PR China

ARTICLE INFO

Keywords:
Fluorometric
Colorimetric
Multi-analytes
Ortho-amino azobenzene

ABSTRACT

In recent decades, researchers have conducted in-depth studies of the design and synthesis of colorimetric/fluorometric probes and the application of such probes to biological and practical samples. The multifunctional colorimetric and fluorescent azo benzene-based probe (4′-hydroxyl-2,4-diaminoazobenzene, **MP**) was designed to detect Al^{3+}, Fe^{3+}, Cu^{2+} and F^-. Based on the distinct redshift of the absorption band and a significant color change (yellow → purple), **MP** was utilized for both naked-eyed and quantitative detection of Al^{3+} and Fe^{3+} after formation of the 1:1 complex. Test paper coated with **MP** and used in conjunction with a cell phone was used for colorimetric detection of Al^{3+} and Fe^{3+} ions (20 μM–2.0 mM) in water samples through naked-eye and digital image colorimetry. The "**MP**-Fe^{3+}" coordination shift that occurs in the presence of the competitive ligand F^- was used in the colorimetric measurement of F^- in toothpaste. In the presence of Cu^{2+} ion, the non-emissive **MP** has transformed into fluorescent benzotriazole product **PMP** ($\Phi = 0.53$) through the bimolecular rate-limiting step, and the second-order rate constant k is calculated as $31 \pm 2\ M^{-1}\ s^{-1}$. **MP** exhibits a "turn-on" fluorescence response in the presence of Cu^{2+} that is greater than its response in the presence of competitive species such as Fe^{3+}, Al^{3+}, Co^{2+}, Fe^{2+}, Zn^{2+}, Cd^{2+}, Mg^{2+}, Mn^{2+}, Ni^{2+} and Ag^+. **MP** was shown to have low toxicity to living HeLa cells and to present good imaging characteristics for tracking of Cu^{2+} in vivo.

1. Introduction

Metal cations and anions are vitally necessary in many physiological processes, in daily life, and in industrial production, and the levels at which they are present may have a profound impact on normal events [1, 2]. In the past two decades, numerous chemosensors that possess the merits of simplicity, low cost, high sensitivity, selectivity, and applicability to on-site analysis through spectral technology have been designed for the detection of metal cations and anions [3, 4, 5, 6, 7, 8]. From the perspective of practical application, the detection of multiple analyses with a single chemosensor would be more effective and economical than the use of many individual analysis procedures [9, 10], and the studies on recognition of multiple target species, including tri- or tetra-ions, are still urgently needed. Aluminum ion (Al^{3+}) as the third most abundant element in the Earth's crust are found everywhere in our daily life, however, the high concentration of Al^{3+} in the environment is toxic, and this causes many health problems, such as Alzheimer's disease and Parkinson's disease. Moreover, iron ions (Fe^{3+}) and copper ions (Cu^{2+}) play the irreplaceable role in many fundamental physiological processes in organisms. In fact, more than 2/3 of the body's iron can be found in blood and muscle cells in the forms of hemoglobin and myoglobin. Cu^{2+} ions are involved in the process of iron absorption in the body, and maintenance of an appropriate concentration of Cu^{2+} is useful in maintaining normal bodily functions. The fluorine anion (F^-), as a typical halogen ion, also has a close association with human health. It is widely added to drinking water at concentrations ranging from 2–4 $mg{\cdot}L^{-1}$ to help avoid osteoporosis and dental fluorosis [11]. To date, a certain number of chemosensors that can be used to monitor one or two of these four ions (Al^{3+}, Fe^{3+}, Cu^{2+}, and F^-) have been developed; however, no studies have reported the selective detection of the abovementioned four ions using a single chemosensor.

Recently, considerable effort has been focused on designing fluorescent and colorimetric probes for Cu^{2+} based on azo dyes. These dyes have advantages that include their low cost as industrial colorants, their simple synthesis, and the rich colours they produce [12]. Ortho-substituted azobenzenes, a subgroup of classical azo dyes, can distinguish Cu^{2+} through reversible coordination reaction and through irreversible oxidation process [13, 14, 15, 16, 17, 18]. In the

* Corresponding author.
** Corresponding author.
E-mail addresses: renhong@jlict.edu.cn (H. Ren), wuping@jlict.edu.cn (P. Wu).

https://doi.org/10.1016/j.heliyon.2022.e10216
Received 9 March 2022; Received in revised form 15 June 2022; Accepted 2 August 2022
2405-8440/© 2022 The Authors. Published by Elsevier Ltd. This is an open access article under the CC BY-NC-ND license (http://creativecommons.org/licenses/by-nc-nd/4.0/).

development of chemosensors belonging to the ortho-amino azobenzene family, three different strategies have been applied. The first strategy is the introduction of electron-donating groups, such as alkyl or amine group onto the ortho substituted azobenzene, which can accelerate the oxidative cyclization reaction by trace Cu^{2+} ions in neutral water solution [13]. The second strategy is related to inner ligand method, which served as a powerful tool in activation of C–H bonds for constructing C–C bonds [19, 20]. A third strategy is introduction of multifunctional groups in o-(phenylazo)aniline based molecular probes, such as Si–O groups in which the Si–O bond is broken due to the effect of F^-; a bifunctional probe for Cu^{2+} and F^- was designed using this method [21]. Furthermore, chemical equilibrium has been applied to quantitative analysis, for example, through the use of S^{2-} [22,23], the introduction of which alters the spectral and electrical signals produced by coordination compounds.

Inspired by the above three strategies, which can be used to design chemosensors based on the o-(phenylazo)aniline platform and on the principle of chemical equilibrium, a multifunctional azobenzene probe (4′-hydroxyl-2,4-diaminoazobenzene, **MP**) for Fe^{3+}, Al^{3+}, Cu^{2+} and F^- is studied in this paper. The work presented here focuses on the spectral characteristics, mechanisms, and applications of **MP**. The hydroxyl and amino groups in **MP** act as internal ligands and influence the density of the electron cloud in the benzene ring. The interaction of **MP** with Fe^{3+}, Al^{3+} ions based the coordination reaction indicating both changes of naked eye color and UV/Vis spectra. The determination of F^- has been achieved by the movement of chemical equilibrium, in which F^- was severed as the competitive ligand of "**MP**-Fe^{3+}" complex. High selectivity and sensitivity of **MP** towards Cu^{2+} was achieved by synthesis of the highly fluorescent product 2-(4-hydroxylphenyl)-2H-benzo[d] [1, 2, 3] triazol-5-amine (**PMP**) during the Cu^{2+}-catalytic process. Test paper coated with **MP** can be used in a pure water system for field determination of the levels of Fe^{3+} and Al^{3+} ions. The "**MP**-Fe^{3+}" complex could also be a reliable probe for the quantitative determination of F^- in toothpaste. **MP** has been studied in HeLa cells by confocal fluorescence microscopy and shown to allow fluorescence imaging and successful tracking of Cu^{2+} levels in vivo. The spectral characterization, mechanism of action, and application of **MP** in three different modes are summarized in Scheme 1.

2. Results and discussion

2.1. Colorimetric analysis of Al^{3+} and Fe^{3+} using MP

The colorimetric abilities of **MP** with different metal ions were investigated by UV/Vis spectroscopy. The free **MP** shows the strong absorption band at 439 nm, which can attribute to the azo chromophore with molar absorption coefficient $\varepsilon_{439\ nm} = 2.49 \times 10^4\ L\ mol^{-1}{\cdot}cm^{-1}$ (R^2 = 0.9990) (Figure 1). Addition of Fe^{3+} and Al^{3+} induced an apparent spectral change, whereas other ions like Co^{2+}, Fe^{2+}, Zn^{2+}, Cd^{2+}, Mg^{2+}, Mn^{2+}, Ni^{2+}, Ag^+ and Cu^{2+} did not cause any obvious variations. Accompanied by the addition of Fe^{3+}, Al^{3+} ions to the **MP** solution with molar ratio 1:1, the color of mixture changed from yellow to light-purple rapidly, and the purple solution can be stable over 20 days in atmosphere. The Fe^{3+}, Al^{3+} ion recognition behaviors of **MP** were also investigated by UV/Vis spectroscopy with the addition of various cations concentrations to **MP** solution, and the ratio metric decrease of the band focused at ~439 nm and increase at ~487–489 nm (Fe^{3+} 487 nm, Al^{3+} 489 nm) with the isosbestic point at ~447 nm. The formation of "M^{n+} + **MP**" complex (M^{n+} = Fe^{3+}, Al^{3+}) were proved by the red shift and good defined isosbestic point. As shown in the UV/Vis spectra, the large red shift for **MP** may be due to extensive delocalization of electrons with addition of metal ions that decreased the required energy for transition.

As the plot of absorbance **MP** vs Fe^{3+}, Al^{3+} concentration (5–15 μM for Fe^{3+}, 5–20 μM for Al^{3+}) showed a good linear relation, the quantitative detection of Fe^{3+}, Al^{3+} through UV/Vis spectra is possible (Figures 2 and 3), and the limit of detection (LOD) is 2.36 μM for Al^{3+}, and 2.68 μM for Fe^{3+}. The patterns of UV/Vis spectra remain largely unchanged with addition of more than 1.0 eq of metal ions. The Benesi–Hildebrand equation are introduced to calculate the binding constant k of "M^{n+} + **MP**" complex. The functional relationship between the $1/(A-A_0)$ and $1/[M^{n+}]$ has been established with the perfect linear relationship, providing evidence of 1:1 stoichiometry between **MP** and Fe^{3+} with k of $7.46\times10^4\ M^{-1}$, and k for Al^{3+} is $6.80\times10^4\ M^{-1}$. The value of binding constant k has indicated that Fe^{3+}, Al^{3+} and **MP** combinate to a large extent, and the concentration of "M^{n+} + **MP**" complex in the solution is dominant compared with Al^{3+}, Fe^{3+} and free **MP** (Fig 4a-b).

To give insight of the response ability between **MP** and Fe^{3+}, Al^{3+}, the addition of EDTA to "M^{n+} + **MP**" (M^{n+} = Fe^{3+}, Al^{3+}) system indicated that the sensing process of MP with Fe^{3+}, Al^{3+} was reversible in the present of EDTA (Figures 2 and 3), reflecting the coordination interaction mechanism between ions with **MP** [24, 25, 26]. Combined with the results of UV/Vis spectra titrations, EDTA cycle experiment, and calculation of binding constant k, the coordination mechanism and mode between **MP** and Fe^{3+}, Al^{3+} ions are proved sufficiently.

The energy-optimized structures of **MP** and the "M^{n+} + **MP**" complex were studied using the Gaussian 16 program (M^{n+} = Fe^{3+}, Al^{3+}). Geometry optimization calculations for C, H, O and N were performed by using the B3LYP DFT method. The basis set used for the C, H, O and N atoms was 6–311++G (d,p), and the LANL2DZ pseudopotential basis set was employed for Fe and Al atom. Frequency calculations under the same level were performed to determine the nature of a stationary point. The electron distributions and orbital energies of the highest occupied molecular orbital (HOMO) and the lowest unoccupied molecular orbital (LUMO) of chemosensor **MP** and "M^{n+} + **MP**" complex has been given in Figure 5. From the point of energy, the energy gap between the HOMO (−15.800 eV) and LUMO (−13.684 eV) of "Fe^{3+} + **MP**" complex was calculated to be 2.116 eV, and the energy gap for Al^{3+} are 2.387 eV, indicating the formation of complex has reduced energy of mixture and stabilized the system corresponding the red shift in UV/Vis spectroscopy. The azo and amino group served as the coordinate sites in constructing the "M^{n+} + **MP**" complex, afforded information on the coordination behavior between **MP** and metal ions.

In order to expand the scope of application, the colorimetric test paper experiment was carried out with **MP** [27]. The filter papers coated with **MP** (5.0 mM) could detect Fe^{3+}, Al^{3+} with minimum concentration of 20 μM together with color change from yellow to purple and distinguish them from other metals. With increasing the concentration of Fe^{3+} and Al^{3+} ions (20 μM–2.0 mM), the color of the test paper strips changes by degrees (Figure 4c). The paper sensor treaded with **MP** can be used in

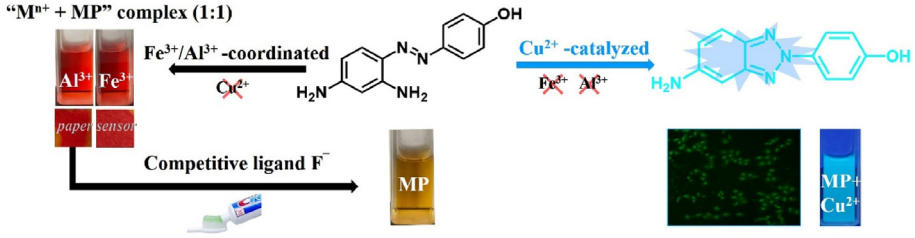

Scheme 1. Multi-functional probe **MP** based on different modes for visual colorimetric and fluorometric sensoring multiple analytes (Al^{3+}, Fe^{3+}, Cu^{2+} and F^-).

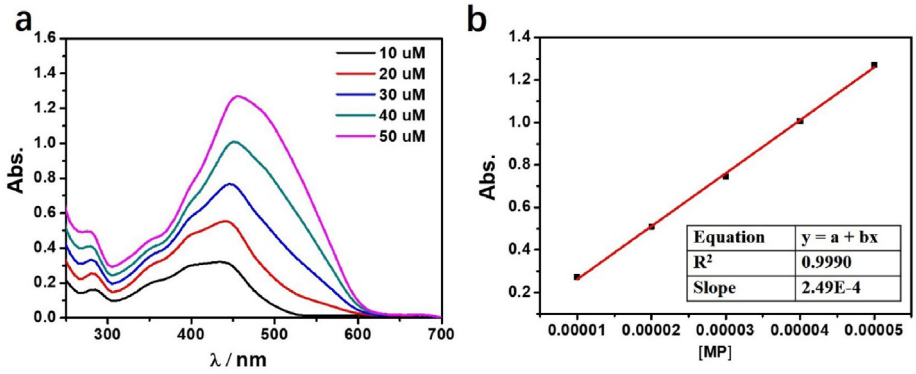

Figure 1. (a) The UV absorbance spectra of different concentrations of **MP** in EtOH solution at room temperature; (b) The function relationship between Abs vs different concentrations of **MP** at 439 nm.

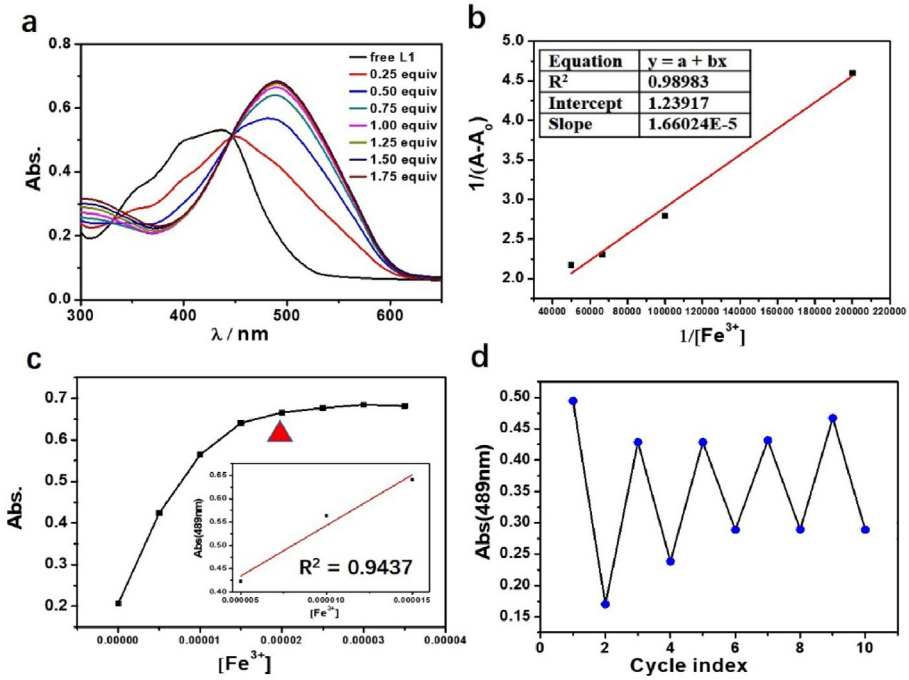

Figure 2. (a) UV/Vis spectra titrations of **MP**(20 μM) with gradually increasing of Fe^{3+} ion; (b) The function relationship between $1/(A-A_0)$ and $1/[Fe^{3+}]$; (c) The relationship of Abs. vs different concentrations of the Fe^{3+} ion, and the red triangle represents that the quantitative relationship between Fe^{3+} and **MP** is 1:1; Insert figure: the good linear relationship between the Fe^{3+} ion concentration (5–15 μM) and Abs. at 489 nm; (d) UV/Vis absorption of **MP** (20 μM) solution circulated with addition of EDTA and Fe^{3+} by turns.

100% aqueous solution for rapid visual detection of Fe^{3+}, Al^{3+}, serving as an ideal naked-eye sensor for on-site assays.

For Fe^{3+} and Al^{3+} ion exist widely in the environment, a convenient, low cost and fast method for Fe^{3+} and Al^{3+}detection in water quality control is highly necessary. Nowadays, cellphone provides portability and accessibility, and there is no demand on the skills of user. Integrating the colorimetric test paper with the cellphone will prompt the quantitative sensing of Fe^{3+} and Al^{3+} based on the RGB color values through color analyzing APP. In detail, we take photos of the colorimetric test paper immersed with a series of concentration (20 μM–2.0 mM) of Fe^{3+} and Al^{3+} which have been added in the tap water in advance. Then the colors of test paper are analyzed, the linear relationship of R/G (red/green) ratios and ion concentrations are built with satisfactory R^2 value (Figure 4d,e).

2.2. Colorimetric studies of the interaction of "MP + M^{n+}" complex with F^- ions

During the past decade, a great deal of probes for detecting F^- ion have been reported based on diverse mechanism such as Lewis's acid-base combination, hydrogen bonding and so on. For example, desilication reaction has been introduced to detect F^- ion with high selectivity, and many probes have been designed to detect F^- ion due to the fracture of C–Si, O–Si and O–P bond [28, 29, 30]. Moreover, the sulfonamide-conjugated poly-(phenylacetylene)s have been prepared to afford a novel colorimetric probe for F^- ion through Lewis acid-base interaction [31]. Nevertheless, most of the F^- probes reported works in organic solution system and the source of F^- is tetrabutylammonium fluoride (TBAF) [32]. In short, detecting F^- using NaF as sources in pure water sample still face challenging for the small atomic radius and high electronegativity of fluorine.

The coordinate interaction between fluoride ions and hard metal ions is strong according to hard and soft acid base theory (such as $[FeF_6]^{3-}$ and $[AlF_6]^{3-}$), and it has been proved that the interactions between hard metal ions and F^- would break the metal-ligand coordination bond [33]. To study the binding properties of "M^{n+}-**MP**" ($M^{n+} = Fe^{3+}$, Al^{3+}) with F^-, UV/Vis spectra titration was performed (Figures 6 and 7). With the molecular ratio of F^- and M^{n+} is equal to 1:1, the absorbance increased at 439–449 nm and decreased at ~555 and ~487 nm, which indicates the recovered to original position of ligand from the reaction of "M^{n+}-**MP**" with F^- along with the color change from purple to yellow. This dissociation can be explained by the stronger binding affinity between F^- and Fe^{3+}, Al^{3+} than the metal-**MP** interaction ($K_f^{\theta}[AlF_6]^{3-} = 6.9 \times 10^{19}$, $K_{f1}^{\theta}[FeF]^{2+} = 7.1 \times 10^{6}$ and $K_{f2}^{\theta}[FeF_2]^{+} = 3.8 \times 10^{11}$), which is much bigger than binding constant k with **MP** (k for Fe^{3+} is 7.46×10^4 M^{-1}, and k for Al^{3+} is 6.80×10^4 M^{-1}). In briefly, the reaction between "M^{n+}-**MP**"

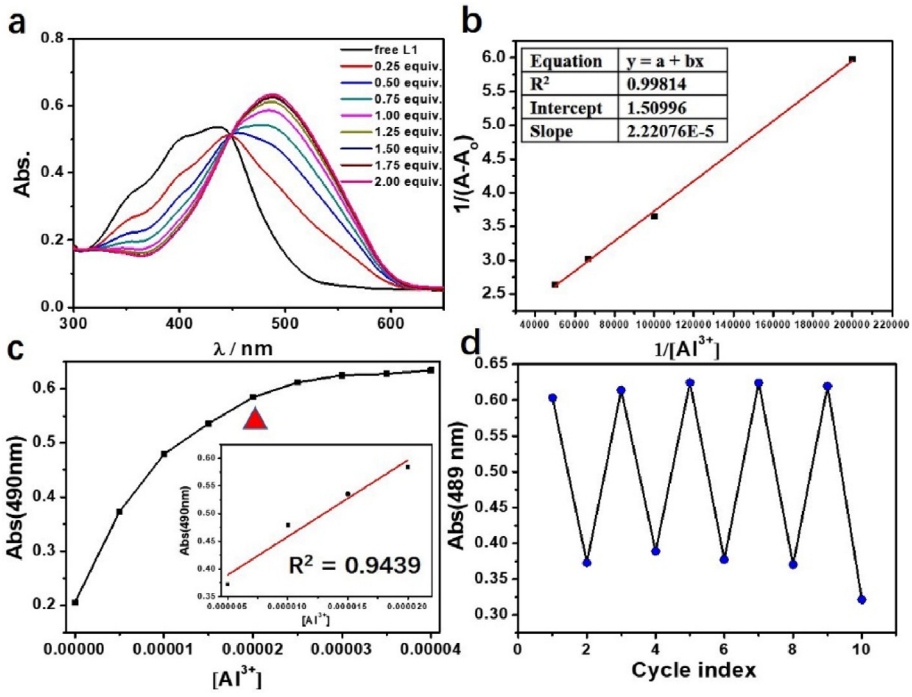

Figure 3. (a) UV/Vis spectra titrations of **MP** (20 μM) with gradually increasing of Al^{3+} ion; (b) The function relationship between $1/(A-A_0)$ and $1/[Fe^{3+}]$; (c) The relationship of Abs. vs different concentrations of the Al^{3+} ion, and the red triangle represents that the quantitative relationship between Al^{3+} and **MP** is 1:1; Insert figure: the good linear relationship between the Al^{3+} ion concentration (5–20 μM) and Abs. at 490 nm; (d) UV/Vis absorption of **MP** (20 μM) solution circulated with addition of EDTA and Al^{3+} by turns.

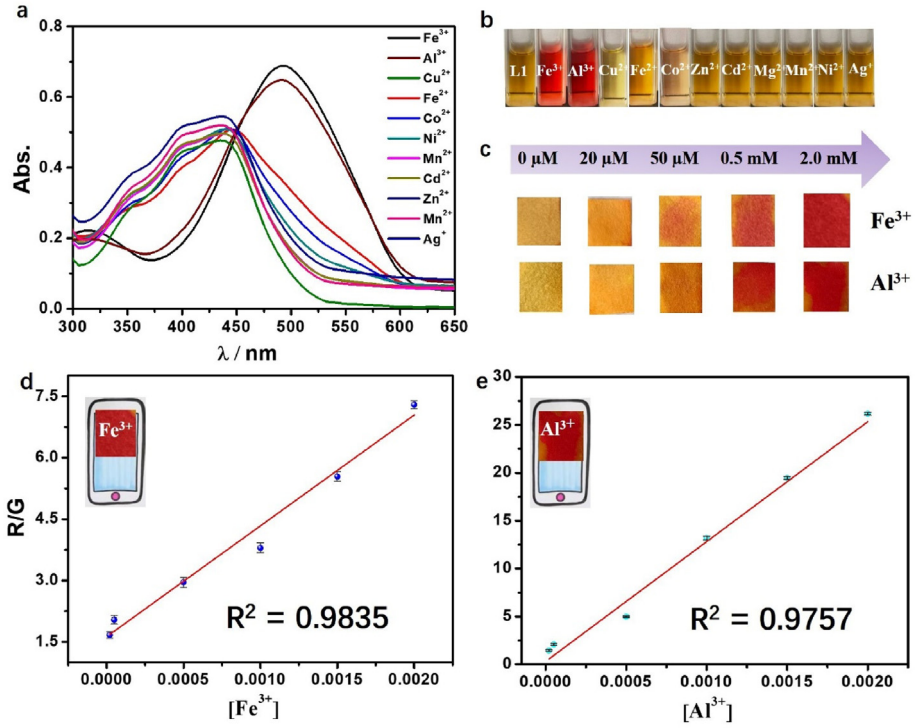

Figure 4. (a) UV absorption spectra of **MP** (20 μM) in the presence of 20 μM different cations (Fe^{3+}, Al^{3+}, Co^{2+} Fe^{2+}, Zn^{2+}, Cd^{2+}, Mg^{2+}, Mn^{2+}, Ni^{2+}, Ag^{+} and Cu^{2+}); (b)The colour change of **MP** with 11 kinds of cations. (c) Yellow paper treated with **MP** (5.0 mM) turn into purple paper in the exist of Fe^{3+}, Al^{3+} ion (20 μM–2.0 mM). (d–e) Digital image colorimetry for Fe^{3+}, Al^{3+} detection based on **MP** test paper using Redmi Note 10 cellphone.

with F^{-} can be attributed to the ligand substitution reaction, in which the F^{-} coordinate with Fe^{3+}, Al^{3+} instead of **MP** ligand.

Moreover, we focused the studies on the complex "**MP**-Fe^{3+}", the inhibition test of "**MP**-Fe^{3+}" towards F^{-} was conducted with a number of anions (Cl^{-}, Br^{-}, I^{-}, CrO_4^{-}, PO_4^{3-}, NO_2^{-}, $S_2O_3^{2-}$, SCN^{-} and AC^{-}) (Figure 6b). With the UV/Vis spectra titration, the complex "Fe^{3+}-**MP**" can detect F^{-}, showing the good linear relationship in a certain concentration range (2.5–15.0 μM). By introducing competitive coordination ions to affect the equilibrium of "**MP**-Fe^{3+}", the detection working curse for F^{-} ion was established successfully. To prove whether the "**MP**-Fe^{3+}" complex could determine fluoride content in authentic specimen, we compared the F^{-} content in Crest® brand toothpaste with detected value, as calculated from weight of toothpaste, respectively. The results shown that "**MP**-Fe^{3+}" complex can be used to determine F^{-} in the toothpaste. Tagged and

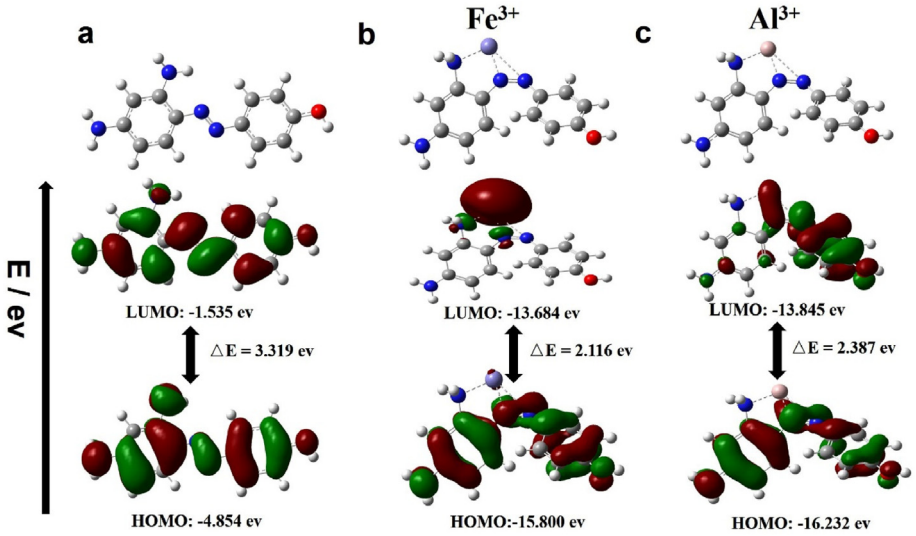

Figure 5. Energy-optimized structures and energy diagram of HOMO and LUMO orbitals for (a) **MP**; (b) "Fe^{3+} + **MP**" (c) "Al^{3+} + **MP**".

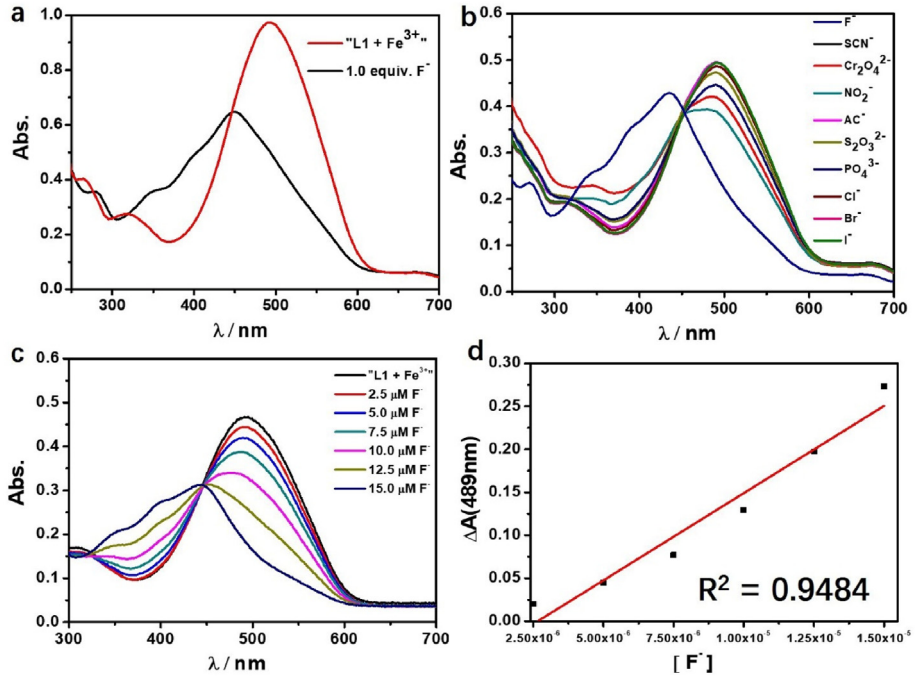

Figure 6. (a) The UV/Vis spectra of "**MP** + Fe^{3+}" complex (Molar ratio = 1:1) with addition of F^-. (b) Absorption of "**MP** + Fe^{3+}" complex adding with a series of anions (F^-, Cl^-, Br^-, I^-, CrO_4^-, PO_4^{3-}, NO_2^-, $S_2O_3^{2-}$, $SCN^-$and AC^-). (c) Absorption of "**MP** + Fe^{3+}" complex with the addition of F^-. (d) Working curve of F^-(2.5–15.0 μM) at 489 nm.

found F^- concentration represented recovery percentage in range of 104.1–116.4% (Table 1). The F^- ion concentration in practical samples such as mouthwash, tap water and groundwater from different areas could be analyzed by the method established by "**MP**-Fe^{3+}" complex toward F^- ion [34].

2.3. Fluorescence spectral response of MP to Cu^{2+} ion

Far different from Fe^{3+} and Al^{3+}, Cu^{2+} ion has not immediately caused the color change of **MP** solution, but the color of the solution began to lighten after 10 min, and the solution faded to colorless within 24h, while the non-emissive **MP** solution has shown strong blue-green light under UV lamp, hence we have carried out the research on fluorescence properties of **MP** with Cu^{2+} (Figure 8). When 0.50 to 8.0 equivalents of Cu^{2+} ion were added to **MP** solution, an obvious bright blue fluorescence at about 460 nm induced, which is far different from of initial **MP** solution. The fluorescence emission intensity of **MP** exhibited a good linear relationship with the concentration of Cu^{2+} (0.50–8.0 μM) and LOD of **MP** for Cu^{2+} ion was determined to be 0.959 μM through 3σ/*k* method, which is far less than the maximum allowable concentration 31.5 μM of Cu^{2+} in potable water as set by the WHO [10]. The selectivity of the **MP** was investigated by preparing a series of metal ion solutions (Fe^{3+}, Al^{3+}, Co^{2+}, Fe^{2+}, Zn^{2+}, Cd^{2+}, Mg^{2+}, Mn^{2+}, $Ni^{2+}$and Ag^+), and then added separately to the **MP** (1.0 μM) solution. It is observed that only addition of Cu^{2+} (1.0 μM) caused the apparent fluorescence enhancement of **MP** solution, while other metal ions cause no significant changes. In order to prove the anti-interference of probe, a competing experiment was performed by the addition of Cu^{2+} (1.0 μM) in the

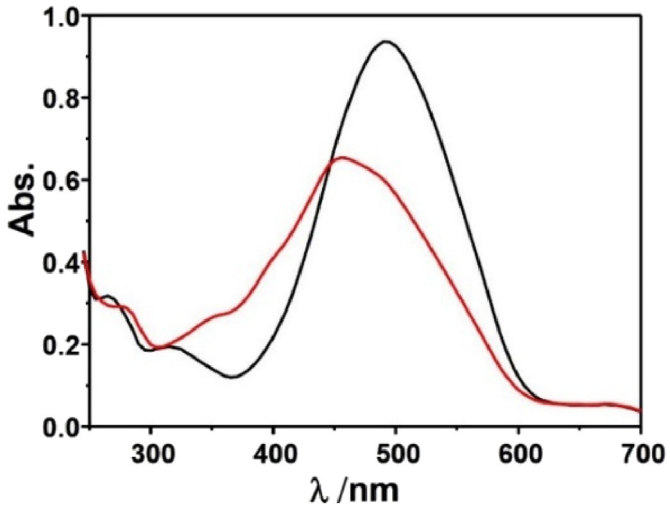

Figure 7. The UV absorbance spectra of "**MP** + Al^{3+}" complex (Molar ratio = 1:1) with addition of F^-.

Table 1. Determination of F^- in toothpaste samples.

Sample	F^- tagged (μM)	F^- found (μM)	Recovery (%)
1	5.80	5.85	104.1%
2	11.6	13.5	116.4%
3	17.4	18.8	108.0%

presence of other species with molecular ratio as 1:1. For **MP**, the metal ions Fe^{3+}, Al^{3+}, Co^{2+} Fe^{2+}, Zn^{2+}, Cd^{2+}, Mg^{2+}, Mn^{2+}, and Ni^{2+} give no disturbance with Cu^{2+}. For the merits of high selectivity, anti-interference and rapid response, the application of **MP** could determine Cu^{2+} instantly in environmental and biological systems.

The fluorescent probes including two basic mechanisms for achieving specificity has been designed: (1) Cu^{2+}-coordinated reaction sensing and (2) Cu^{2+}-promoted reaction sensing [35]. In both types, a fluorescent chemosensor consists of a molecule incorporating an ion-binding site and fluorophore, and the sensing process can be concluded as the target metal analyte attached to the fluorophore affect the change of fluorescence. The coordinating-based type depends on a chelating ligand that reversibly binds the targeted metal and induces a fluorescence response through mechanisms containing internal charge transfer (ICT), photoinduced electron transfer (PET), and Förster resonance energy transfer (FRET). The fluorescence recognition process is usually reversible by adding other chelating reagents (EDTA or critic acid [36]) For the other type, the activity-based sensing trend to utilize the specific transformations induced by specific metal, the Cu^{2+}-promoted reaction sensing involved the irreversible chemical reactions in which the non-emissive reactants transform to fluorescent products. The Cu^{2+} ion probes based on azobenzene can served both as Cu^{2+}-coordinated and Cu^{2+}-promoted reaction sensing [15, 17]. In this paper, N=N isomerization of **MP** were prevented in the present of Cu^{2+}, and the Cu^{2+}-catalyzed oxidation mechanism is recommended (Scheme 1). To prove **MP** as Cu^{2+}-promoted reaction sensing, the fluorescent product (**PMP**) was prepared directly and fully charactered. The emission peak of **PMP** is around 460 nm, which coincides with the position of "**MP** + Cu^{2+}" in fluorescent spectra (Figure 9). Using quinine sulfate as reference, the fluorescence quantum yields Φ of **PMP** have been measured (Φ = 0.53). Owing to the irreversible Cu^{2+} catalysis process, the addition EDTA to "**MP** + Cu^{2+}" mixture has not changed the fluorescence emission as predicted (Figure 10a). With the molecular ratio of F^- and Cu^{2+} is equal to 1:1, the fluorescence properties of "**MP** + Cu^{2+}" mixture has remained the same under the UV lamp (Figure 10b). The mixture solution of "**MP** + Cu^{2+}" was analyzed by HR-Mass, a peak of 227.09 (m/z) was suggestive to be $[\mathbf{PMP}]^+$ [calcd. 229.24]. The strong peaks of reactants **PMP** demonstrated that **MP** has been converted into **PMP** completely, the **MP** as the Cu^{2+}-promoted reaction sensing has been fully proved (Figure 11).

The systematic kinetic studies between reactants **MP** and Cu^{2+} have been carried out. We concluded by the evidence that the reaction between the **MP** and Cu^{2+} proceeds at room temperature to provide a highly fluorescent product **PMP**. We set that Cu^{2+} reactant was greatly excessive (≥300 equiv of $[Cu^{2+}]$ with respect to **MP**), and its consumption in the reaction was negligible relative to **MP**. The generation of the product **PMP** was monitored by time-dependent enhancement in the fluorescence intensity at 465 nm under pseudo-first-order reaction condition. Using Eq. (1), the exponential increase in $\Delta I_{465\ nm}$ as a function of time was fitted to calculate the pseudo-first-order rate constant k':

$$\frac{\Delta I}{I} = 1 - e^{-k't} \qquad \text{eq 1}$$

Furtherment, the linear dependence of k' (= k $[Cu^{2+}]_o$; eq 1) on $[Cu^{2+}]_o$ established that the reaction proceeds via bimolecular rate-limiting step with first-order in both Cu(II) ion and **MP**, and the second-order rate constant is calculated as $k = 31 \pm 2\ M^{-1}\ s^{-1}$, which is slightly bigger than the azobenzene-based probes reported [13]. It is also shown that the accelerating effect of inner ligand effect on cyclization reaction [20] (Figure 8).

Given that the probe **MP** senses Cu^{2+} with fluorescence enhancement, we further used it for the cellular imaging. The Hela cells were alive with high OD value (92.6%) with 250 μM **MP** incubated in cells for 24 h according to the CCK8 method, suggesting that **MP** has no toxicity to cells. Subsequently, Hela cells incubated with the probe (50 μM, aqueous solution) for 30 min, and then were washed with PBS solution for three times. The cells were further incubated with Cu^{2+} (5 mM). The strong fluorescence can be seen after Hela cells pretreated by **MP**. By contract, Hela cell remained non-emissive only in the presence of Cu^{2+} or **MP**. During the reaction process, the morphology of cells was not damaged which is consistent with the results of CCK8. The results indicated that the **MP** offered a reliable detection method to intracellular Cu^{2+} by fluorescence imaging (Figure 12).

2.4. Comparison of MP with other chemosensors

In this paper, **MP** served as a chemosensor for multiple targets. The **MP** coordinated with Fe^{3+} and Al^{3+} ions, resulting in changes in colour visible to the naked eye and changes in the UV/Vis spectra. The coordination equilibrium of "**MP**-Fe^{3+}" can shift due to binding of the competitive ligand F^-. Although **MP** is nonfluorescent, a fluorophore can be released via Cu^{2+}-promoted oxidative cyclization to the benzotriazole product **PMP**. A comparison of **MP** with other reported chemosensors is given in Table 2. Although fluorescence detection is more sensitive than UV/Vis detection, the LODs of Fe^{3+}, Al^{3+} and F^- for **MP** are close to or better than those of fluorescent probes [37, 38, 39, 40]. The LOD of Cu^{2+} for **MP** reaches a level that is above average among chemosensors based on small organic molecules [22, 23, 38, 39], allowing it to be used to test conformity to the standard for drinking water established by WHO (≤31.5 μM). Moreover, EtOH, the solvent used in the **MP** sensing system, has relatively lower toxicity than other solvents. Thus, **MP** has expanded the scope of applications to water quality detection, daily chemical analysis, and biology.

3. Conclusion

The azobenzene-based chemosensor **MP** was developed for effective use in colorimetric recognition of Al^{3+} and Fe^{3+} through a coordination mechanism and sequential sensing of F^- through an equilibrium-shift mechanism. For Cu^{2+} ion recognition, efficient chemical transformation was obtained using azo dye transfer to the fluorescent benzotriazole **PMP**. Through combined UV/Vis spectra titration, analysis of

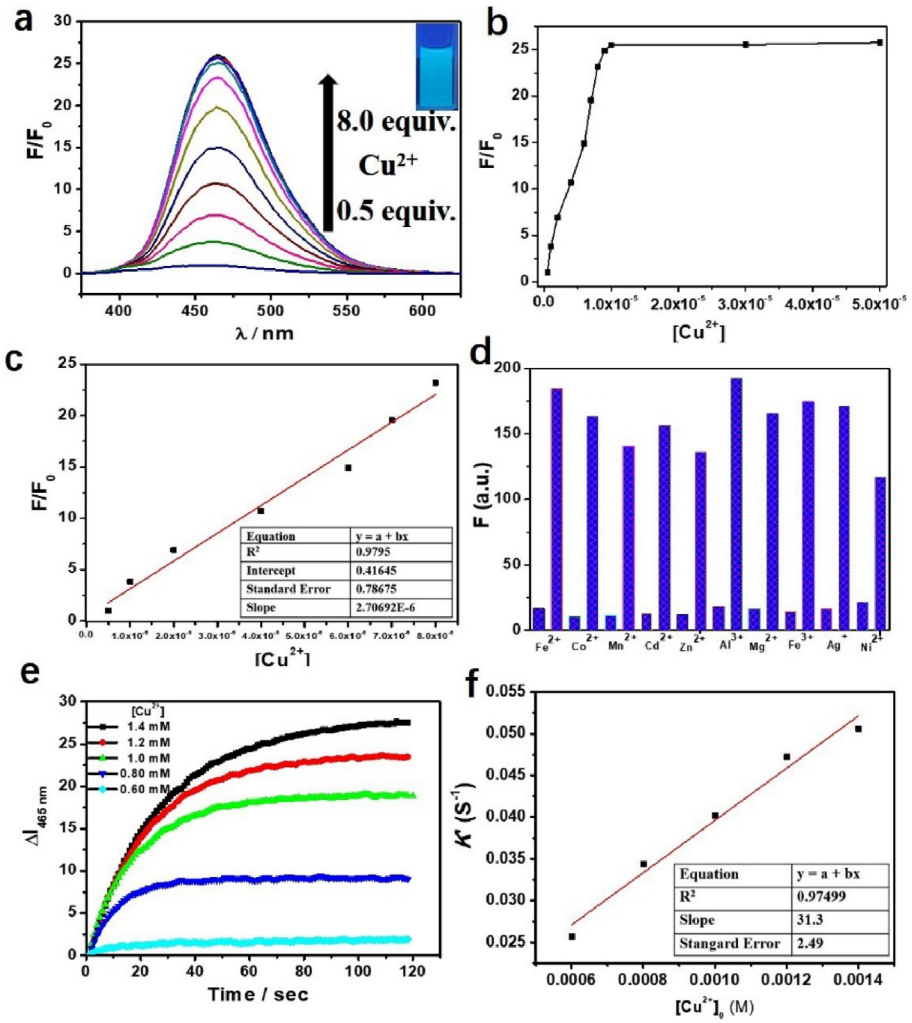

Figure 8. (a) Fluorescence spectra of **MP** (1.0 μM) and Cu^{2+} (0.5–8.0 equiv). Insert: the mixture of **MP** and Cu^{2+} under UV lamp. (b) The fluorescence intensity vs Cu^{2+} ion concentrations at ~460 nm. (c) The linear relationship of fluorescence intensity vs Cu^{2+} ion (0.5–8.0 μM). (d) Fluorescence intensity changes of the **MP** (1.0 μM) to Cu^{2+} (1.0 μM) with interfering ions (1.0 μM) at ~465 nm (Lower: Interfering ion; Higher: Interfering ion + Cu^{2+} ion). (e) At 465 nm, time-dependent changes in the fluorescence intensity observed for the reaction between **MP** (2.0 μM) and Cu^{2+} (0.60, 0.80, 1.0, 1.2, and 1.4 mM; from bottom to top traces) at room temperature. (f) The linear relationship of k' (= $k[Cu^{2+}]_0$) vs $[Cu^{2+}]_0$ to gain the second-order rate constant $k = 31 \pm 2\ M^{-1}\ s^{-1}$.

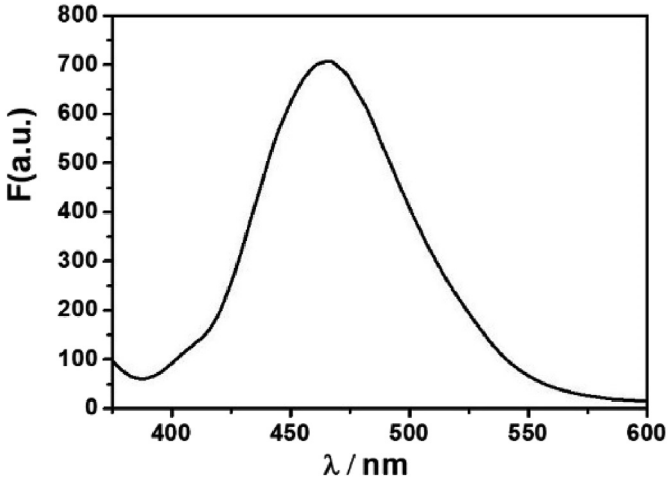

Figure 9. The fluorescence spectra of **PMP** in ethanol solution.

fluorescence spectra, and HR-MS and EDTA chelation studies, we have provided insight into the multianalyte sensing process. **MP** is the first example in which a chemosensor based on an azo dye can simultaneously sense Al^{3+}, Fe^{3+}, Cu^{2+} and F^-. Test paper coated with **MP** can be used to detect Al^{3+} and Fe^{3+} over a wide concentration range through color change (yellow→ purple), and this can be combined with a cell phone system to allow quantitative sensing. The "**MP**-Fe^{3+}" complex was able to detect F^- in a toothpaste sample. Furthermore, **MP** efficiently and selectively recognized Cu^{2+} over other metal ions with high selectivity and sensitivity (LOD = 0.959 μM), as indicated by significant fluorescence enhancement at 460 nm. The successful preparation of test paper and the determination of F^- in toothpaste and Cu^{2+} in HeLa cells using imaging based on **MP** has paved the way for the use of azo dyes in sensing applications related to environmental and biological monitoring and daily life. It is clear that a single probe that can simultaneously detect these four ions (Al^{3+}, Fe^{3+}, Cu^{2+}, and F^-), all of which are closely related to daily life and to human health, will be both attractive and practical. The results indicate that **MP** represents a model for the design of a single chemosensor for multianalytes that can be used in both colorimetric and fluorescent modes.

4. Experimental section

4.1. General information

Most chemicals in this paper were purchased from commercial companies at analytic grade and used without further purification. Fresh double distilled water was used throughout the experiment. UV/Vis spectra were recorded on a Cary 60 spectrophotometer of Agilent Technologies using a 10 mm path length quartz cuvette. Infrared spectra were measured on a Nicolet Impact 410 spectrometer between 400 and 4000 cm^{-1}, using the KBr pellet method. Mass spectra were collected on a Waters Xevo G2-XS QTof spectrometer. The NMR spectra were obtained

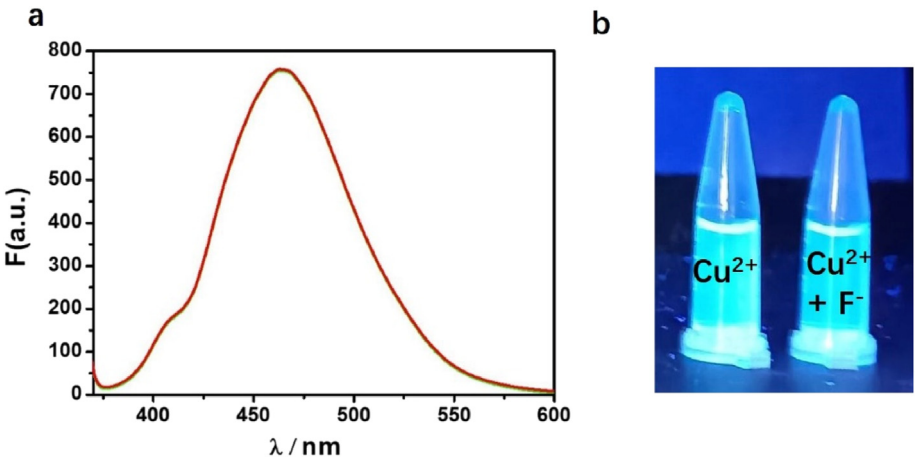

Figure 10. (a) The fluorescence emission spectra of solution of "**MP** + Cu^{2+}" adding with EDTA with same concentration of **MP**. Red line: **MP** + Cu^{2+}; green lines: **MP** + Cu^{2+}+ EDTA. (b) Left: The **MP** (4.0 μM) ethanol solution (0.5 mL) added with Cu^{2+}(4.0 μM); Right: The initial solution of "**MP** + Cu^{2+}" added with F^- (4.0 μM).

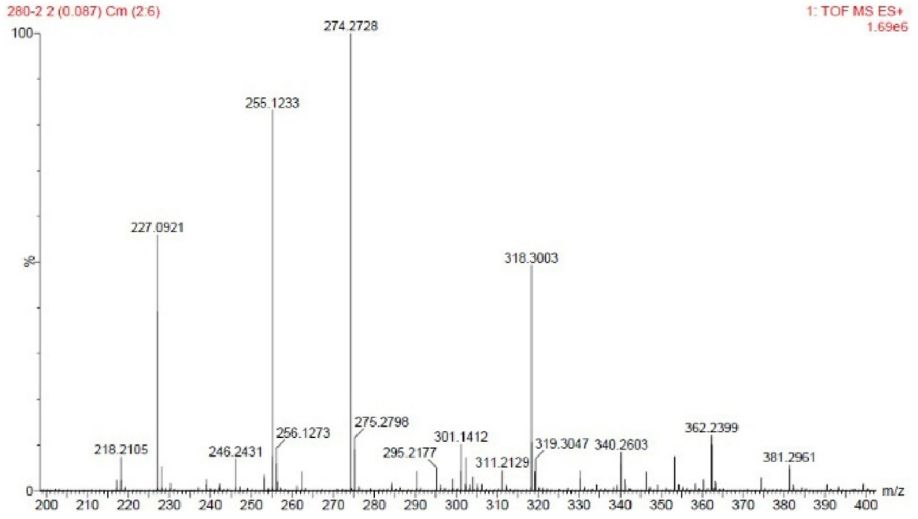

Figure 11. Mass spectra of solution of "**MP** + Cu^{2+}", which has demonstrated the formation of **PMP** for the peak at 227.09.

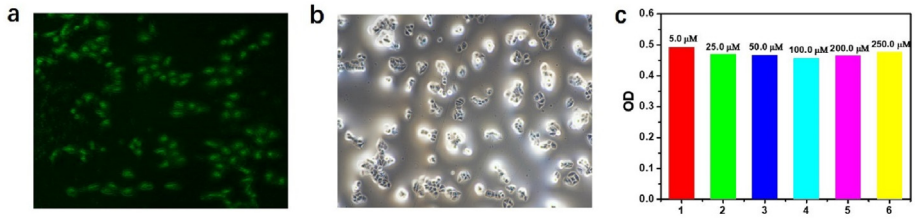

Figure 12. (a) Fluorescence image in green channel of Hela cells preloaded with Cu^{2+} (5 mM) for additional 0.5h. (b) Bright-field image of Hela cells preloaded with probe **MP** (50 μM) in PBS (0.01 M, pH 7.4) for 30 min at 37 °C. (c) The effects of different concentrations of **MP** on the Hela cells by cck8 method for 24 h.

on a Bruker-400 spectrometer, and the chemical shifts are expressed in δ ppm using TMS as an internal standard. The fluorescence data were determined on a PerkinElmer LS 45 luminescence spectrometer. For all luminescence measurement, excitation and emission slit widths of 10 nm were used. The wave number of excited light for UV lamp is 365 nm. The cell experiment was carried out with Nikon eclipse *Ti* microscope.

4.2. Preparation of MP and PMP

The **MP** was prepared using 4-aminophenol and 1,3-phenyldiamine as reactants through classical diazo coupling reaction (Figure 13). Using **MP** as raw material, the **PMP** was prepared under the oxidation of Cu^{2+}. The chemical structure of **MP**, **PMP** were confirmed by ^{1}H NMR, ^{13}C NMR, Mass and IR spectra (Figures 14 and 15). ^{1}H NMR (400 MHz, DMSO-d_6) of **MP**: δ 9.67 (s, 1H), 7.57 (d, J = 8.6 Hz, 2H), 7.32 (d, J = 8.7 Hz, 1H), 6.82 (d, J = 8.7 Hz, 2H), 6.76 (s, 1H), 5.96 (d, J = 6.8 Hz, 1H), 5.87 (s, 1H), 5.70 (s, 2H). ^{13}C NMR (101 MHz, DMSO-d_6) of **MP**: δ 158.00, 148.41, 146.75, 139.59, 132.68, 122.26, 121.41, 118.50, 116.40, 93.18. MS (ES-API) for **MP**: calcd. $C_{12}N_4OH_{13}$ $[M + H]^+$: 229.26; found 229.09. For IR spectra, the peaks at 3341 and 3210 cm^{-1} are corresponding to the hydroxyl group. **MP** Yield: ~85%. ^{1}H NMR (400 MHz, DMSO-d_6) of **PMP**: δ 9.92 (s, 1H), 8.00 (d, J = 8.9 Hz, 2H), 7.66 (d,

Table 2. The comparison of **MP** with other reported chemosensors.

Methods	Target ions	Mechanism types	LOD/μM	Solvent	Application
This paper	Fe^{3+} Al^{3+} F^- Cu^{2+}	Colorimetric; Colorimetric; Colorimetric; Fluorescence.	2.68 2.36 2.5 0.959	EtOH	Paper strip for practical water sample; F^- in toothpaste; Hela cells.
[37]	Al^{3+} F^-	Fluorescence; Fluorescence.	0.19 1.9	Bis–Tris buffer solution (pH = 7.0)	Real water sample, Hela cells; Real water sample.
[38]	Al^{3+} Cu^{2+}	Colorimetric; Colorimetric.	1.07 1.6	EtOH/H_2O	Human lymphocyte cells.
[39]	Cu^{2+} F^-	Fluorescence; Fluorescence.	2.0 2.8	DMF/bis-tris buffer	—
[22]	Cu^{2+}	Colorimetric	7.69	EtOH	Paper strip for practical water sample.
[23]	Cu^{2+}	Fluorescence	0.0767	HEPES buffer	RKO cells.
[40]	Fe^{3+}	Fluorescence	360	Methanol/H_2O	Hela cells.

J = 9.1 Hz, 1H), 6.94 (d, J = 8.9 Hz, 3H), 6.70 (s, 1H), 5.55 (s, 2H). ^{13}C NMR (101 MHz, DMSO-d_6) of **PMP**: δ 158.09, 152.78, 146.93, 146.58, 129.52, 128.25, 122.98, 115.99, 105.50, 97.70. MS (ES-API) for **PMP**: calcd. $C_{12}N_4OH_{11}$ $[M + H]^+$: 227.24; found 227.09. IR spectra for **PMP**, the peak around 1644–1424 cm^{-1} is attributed to benzotriazole ring in products [41]. **PMP** Yield: ~60%.

4.3. General procedure for UV/Vis spectroscopy

4.3.1. Preparation of MP solution for UV/Vis spectroscopy

Add 10, 20, 30, 40 and 50 μL **MP** solution (2.0 mmol L^{-1}) to ethanol solution to obtain the molar absorption coefficient from C-A relationship, and the total volume of ethanol solution was kept as 2.0 mL.

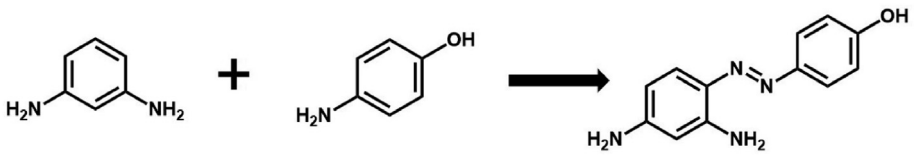

Figure 13. Schematic diagram of synthetic **MP**.

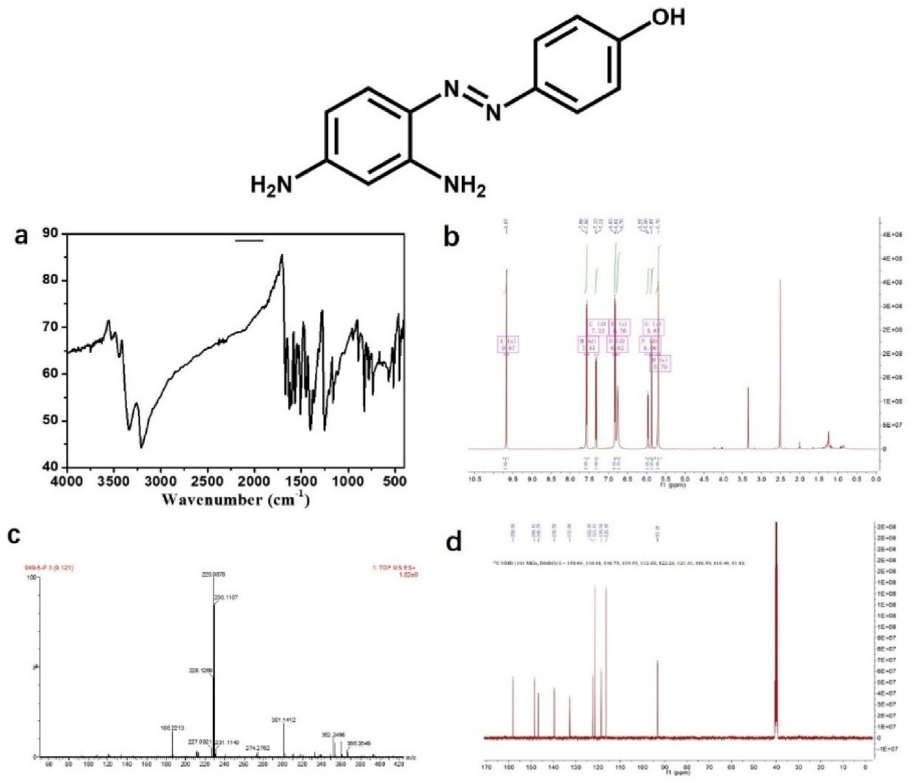

Figure 14. (a) IR (b) ^1H NMR (c) HR-Mass and (d) ^{13}C NMR of **MP**.

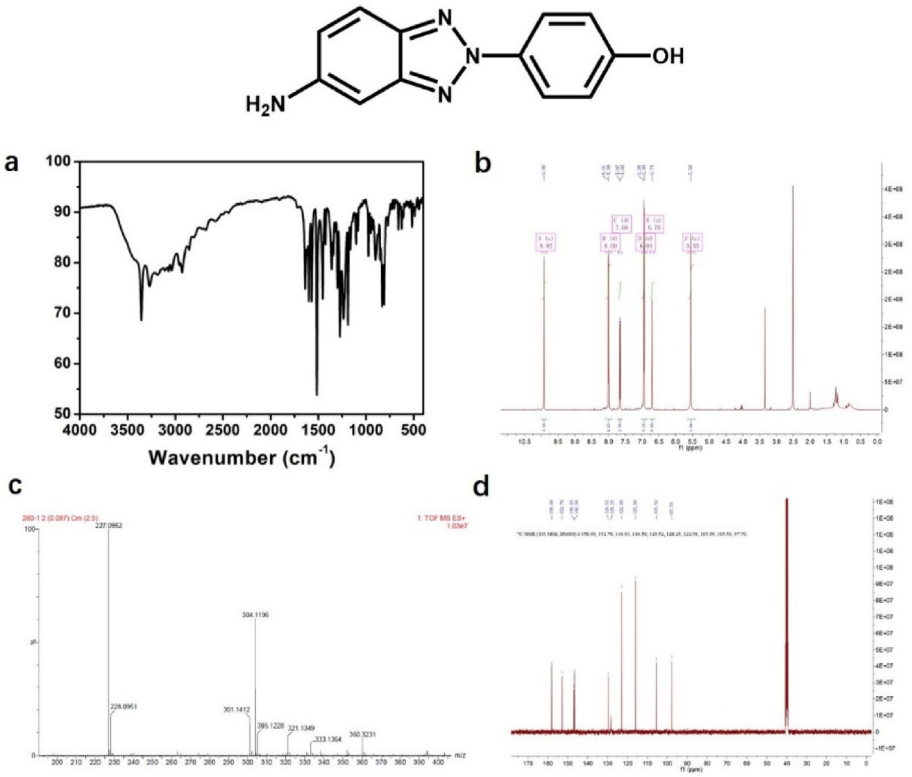

Figure 15. (a) IR (b) ^{1}H NMR (c) HR-Mass and (d) ^{13}C NMR of **PMP**.

4.3.2. UV/Vis spectra titrations

The initial **MP** ethanol solution (20 μM, 2.0 mL) was titrated by addition of Fe^{3+}, Al^{3+} solution (0, 0.25, 0.50, 0.75,1.0, 1.25, 1.50, 1.75, 2.0 equivalents). For other metal salts (Co^{2+}, Fe^{2+}, Zn^{2+}, Cd^{2+}, Mg^{2+}, Mn^{2+}, Ni^{2+}, Ag^{+} and Cu^{2+}), the **MP** solution was added by salt solution (5.0 mM) with 1.0 equivalents once time.

4.3.3. The EDTA chelation experiment

The formation of "M^{n+}-**MP**" complex in ethanol solution can be gained by mixing the Fe^{3+}, Al^{3+} salt (5 mM, 8 μL) and **MP** (2.0 mM, 20 μL) solution. Then the "M^{n+}-**MP**" complex solution was added by EDTA and Fe^{3+}, Al^{3+} salt solution (5 mM), alternately.

4.4. Determination of F^- content in toothpaste

4.4.1. Sample pretreatment of toothpaste

The Crest® toothpaste containing 0.11wt% F^- as labeled was selected. Firstly, the 200 mg toothpaste samples were dried for 10h in oven at 80 °C, then the sample was dissolved in 10 mL water. The above solutions were sonicated for 1 h, balanced for another 24 h, centrifuged at 3000 r/min for 10 min and filtered to get clear solution for measuring.

4.4.2. The F^- titrations experiment

The complex "Fe^{3+} + **MP**" can be gained by mixing the Fe^{3+} salt (5.0 mM, 8 μL) and **MP** (2.0 mM, 20 μL) in ethanol system. Then the "Fe^{3+} + **MP**" solution was added by F^- sample (1.16 mM) step by step which was prepared from toothpaste. The NaF solution (0.50 mM) is used as the standard working curve to calculate the F^- content.

4.5. Colorimetric test paper

The filter paper was immersed with **MP** (~5.0 mM) ethanol solution, then was dried in air. A series of ions (Fe^{3+}, Al^{3+}, Co^{2+}, Fe^{2+}, Zn^{2+}, Cd^{2+}, Mg^{2+}, Mn^{2+}, Ni^{2+}, Ag^{+} and Cu^{2+}) were dissolved in distilled water to furnish 2.0 mM stock solution. The test papers prepared in advance were dipped into in metal ions solution.

4.6. General procedure for fluorescence spectroscopy

All the fluorescence spectroscopy of **MP** were recorded upon the addition of metal salts in ethanol system. Using quinine sulfate as the standard reference, fluorescence quantum yields of **MP** were measured. The quantum yield was determined according to the following equation:

$$Y_u = Y_s \cdot \frac{F_u}{F_s} \cdot \frac{A_s}{A_u} \quad \text{eq 2}$$

Where Φ is the quantum yield, and the Y_u and Y_s represent the fluorescence quantum yield of standard and sample, respectively. F_u and F_S denote the integral fluorescence intensity of the substance to be tested and the reference substance, while A_u and A_s represent the absorbance of the substance to be tested and the reference substance at certain wavelength.

4.7. Cell culture and confocal imaging of Hela cells

In humidified atmosphere of CO_2/air (5: 95%) at 37 °C, Hela cells were cultured in modified Eagle's medium (MEM) supplemented with 10% fetal bovine serum (FBS). Then, the cells (3×10^5/well) were seeded in a 12-well plate for 24 h, and washed with PBS buffer (pH = 7.4). The cells in logarithmic growth stage were detected by CCK8 method, the cell viability was measured according to the **MP** concentration gradient from 5–250 μM after 24 h of cultivation.

Declarations

Author contribution statement

Hong Ren: Conceived and designed the experiments; Wrote the paper.
Fei Li: Performed the experiments.

Shihua Yu: Contributed reagents, materials, analysis tools or data.
Ping Wu: Analyzed and interpreted the data.

Funding statement

This work was supported by the scientific research funds of Jilin Institute of Chemical Technology, the Natural Science Foundation of China (NSFC, No. 22106051), and the education department of Jilin Province (No. JJKH20210240KJ).

Data availability statement

Data included in article/supplementary material/referenced in article.

Declaration of interests statement

The authors declare no conflict of interest.

Additional information

No additional information is available for this paper.

Acknowledgements

The authors are thankful to two graduates LIU Fang and QIU Zhuo for experiment on spectroscopy.

References

[1] D. Wu, A.C. Sedgwick, T. Gunnlaugsson, E.U. Akkaya, J. Yoon, T.D. James, Fluorescent chemosensors: the past, present and future, Chem. Soc. Rev. 46 (2017) 7105–7123.
[2] S.L. Lippard, J.M. Berg, Principles of Bioinorganic Chemistry, University Science Books, New York, 1994. Chapter 6.
[3] V. Dujols, F. Ford, A.W. Czarnik, A long-wavelength fluorescent chemodosimeter selective for Cu(II) ion in water, J. Am. Chem. Soc. 119 (1997) 7386–7387.
[4] D. Udhayakumari, S. Naha, S. Velmathi, Colorimetric and fluorescent chemosensors for Cu^{2+}. A comprehensive review from the years 2013-15, Anal. Methods 9 (2017) 552–578.
[5] S. Liu, Y.M. Wang, J. Han, Fluorescent chemosensors for copper(II) ion: structure, mechanism and application, J. Photoch. Photobio. C 32 (2017) 78–103.
[6] G.C. Liu, Y. Li, J. Chi, N. Xu, X.L. Wang, H.Y. Lin, Y.Q. Chen, Multi-functional fluorescent responses of cobalt complexes derived from functionalized amide-bridged ligand, Dyes Pigments 174 (2020), 108064.
[7] L.M. Carneiro, F.H. Bartoloni, C.F.F. Angolini, A.F. Keppler, Solvent-free synthesis of nitrone-containing template as a chemosensor for selective detection of Cu(II) in water, Spectrochim. Acta A. 267 (2022), 120473.
[8] W.F. Luo, S. Zhang, J. Ye, B.H. Jiang, Q.H. Meng, G.H. Zhang, J.Y. Li, Y.P. Tang, A multimodal fluorescent probe for portable colorimetric detection of pH and it's application in mitochondrial bioimaging, Spectrochim. Acta A. 267 (2022), 120554.
[9] H.Y. Liu, B.B. Zhang, C.Y. Tan, F. Liu, J.K. Cao, Y. Tan, Y.Y. Jiang, Simultaneous bioimaging recognition of Al^{3+} and Cu^{2+} in living-cell, and further detection of F^- and S^{2-} by a simple fluorogenic benzimidazole-based chemosensor, Talanta 161 (2016) 309–319.
[10] A. Tarai, Y. Li, B. Liu, D. Zhang, J. Li, W. Yan, J.F. Zhang, J.L. Qua, Z.G. Yang, A review on recognition of tri-/tetra-analyte by using simple organic colorimetric and fluorometric probes, Coord. Chem. Rev. 445 (2021), 214070.
[11] Y. Zhou, J.F. Zhang, J. Yoon, Fluorescence and Colorimetric Chemosensors for Fluoride-Ion Detection, Chem. Rev. 114 (2014) 5511–5571.
[12] D. Sareen, P. Kaur, K. Singh, Strategies in detection of metal ions using dyes, Coord. Chem. Rev. 265 (2014) 125–154.
[13] J.Y. Jo, H.Y. Lee, W.J. Liu, A. Olasz, C.H. Chen, D.W. Lee, Reactivity-based detection of copper(II) ion in water: oxidative cyclization of azoaromatics as fluorescence turn-on signaling mechanism, J. Am. Chem. Soc. 134 (2012) 16000–16007.
[14] J.Y. Jung, A. Dinescu, A. Kukrek, Synthesis and comparative kinetic study of reaction-based copper(II) probes to visualize aromatic substituent effects on reactivity, J. Chem. Educ. 97 (2020) 533–537.
[15] Q.M. Wang, S.S. Wu, Y.Z. Tan, Y.L. Yan, L. Guo, X.H. Tang, A highly selective, fast-response and fluorescent turn on chemosensor for the detection of Cu^{2+} ions and its potential applications, J. Photochem. Photobiol., A 357 (2018) 149–155.
[16] X.L. Sun, Y.F. Xu, W.P. Zhu, C.S. He, L. Xu, Y.J. Yang, X.H. Qian, Copper-promoted probe for nitric oxide based on o-phenylenediamine: large blue-shift in absorption and fluorescence enhancement, Anal. Methods 4 (2012) 919–922.
[17] H. Ren, P. Wu, F. Li, L. Jin, D.W. Lou, Visual colorimetric and fluorescence turn-on probe for Cu(II) ion based on coordination and catalyzed oxidative cyclization of ortho amino azobenzene, Inorg. Chim. Acta. 487 (2019) 234–239.
[18] H. Ren, P. Wu, F. Li, L. Jin, S.H. Yu, D.W. Lou, Development of a colorimetric and fluorescent Cu^{2+} ion probe based on 2′-hydroxy-2,4-diaminoazobenzene and its application in real water sample and living cells, Inorg. Chim. Acta. 507 (2020), 119583.
[19] L.X. Dai, Ullmann reaction, a centennial memory and recent renaissance-related formation of Carbon-Heteroatom bond, Prog. Chem. 30 (9) (2018) 1257–1297.
[20] S. Rej, Y. Ano, N. Chatani, Bidentate directing groups: an efficient tool in C-H bond functionalization chemistry for the expedient construction of C-C bonds, Chem. Rev. 120 (3) (2020) 1788–1887.
[21] M. Gupta, A. Balamurugan, H. Lee, Azoaniline-based rapid and selective dual sensor for copper and fluoride ions with two distinct output modes of detection, Sens. Actuator. B-Chem. 211 (2015) 531–536.
[22] P. Wu, H. Ren, D.D. Han, L. Jin, L.N. Yan, X.T. Cui, Effects of chemical equilibrium on Cu^{2+} colorimetric probe based on azobenzene with ortho amino and sulfonamide group, J. Mol. Struct. 1244 (2021), 130959.
[23] P. Wang, L.Y. Sun, J. Wu, X.P. Yang, P.C. Lin, M. Wang, A dual-functional colorimetric and fluorescent peptide-based probe for sequential detection of Cu^{2+} and S^{2-} in 100% aqueous buffered solutions and living cells, J. Hazard Mater. 407 (2021), 124388.
[24] B. Kaur, N. Kaur, S. Kumar, Colorimetric metal ion sensors - a comprehensive review of the years 2011-2016, Coord. Chem. Rev. 358 (2018) 13–69.
[25] J. Zhang, Z. Yan, S. Wang, M. She, Z. Zhang, W. Cai, P. Liu, J. Li, Water soluble chemosensor for Ca^{2+} based on aggregation-induced emission characteristics and its fluorescence imaging in living cells, Dyes Pigments 150 (2018) 112–120.
[26] T. Wei, G. Liang, X. Chen, J. Qi, Q. Lin, A functional applied material on recognition of metal ion zinc based on the double azine compound, Tetrahedron 73 (2017) 2938–2942.
[27] K.Q. Fan, X.B. Wang, H.R. Yang, L.J. Gao, G.L. Han, L.M. Zhou, S.M. Fang, Semiquantitative naked-eye detection of Cu(II) with a standard colorimetric card via a hydrogel-coated paper sensor, Anal. Methods 12 (2020) 1561–1566.
[28] P.K. Muwal, A. Nayal, M.K. Jaiswal, P.S. Pandey, A dipyrromethane based receptor as a dual colorimetric sensor for F^- and Cu^{2+} ions, Tetrahedron 59 (2018) 29–32.
[29] P.A. Gale, C. Caltagirone, Fluorescent and colorimetric sensors for anionic species, Coord. Chem. Rev. 354 (2018) 2–27.
[30] Y. Liu, S.Q. Wang, B.X. Zhao, A novel pyrazoline-based fluorescent probe for detecting fluoride ion in water and its application on real samples, RSC Adv. 5 (2015) 32962–32966.
[31] R. Sakai, E.B. Barasa, N. Sakai, S. Sato, T. Satoh, T. Kakuchi, Colorimetric detection of anions in aqueous solution using poly(phenylacetylene) with sulfonamide receptors activated by electron withdrawing group, Macromolecules 45 (2012) 8221–8227.
[32] G. Kim, B. Suh, C. Kim, A naked-eye sulfonamide-based colorimetric and fluorescent "turn-on" chemosensor for detecting fluoride, J. Mol. Struct. 1254 (2022), 132307.
[33] Y.P. Ren, J. Han, Y. Wang, X. Tang, L. Wang, L. Ni, An OFF-ON-OFF type fluorescent probe based on a naphthalene derivative for Al^{3+} and F^- ions and its biological application, Luminescence 33 (2018) 15–21.
[34] P. Yadav, H. Laddha, M. Agarwal, H.S. Kushwaha, R. Gupta, Studies on 1,8-naphthalimide derivative as a robust multi-responsive receptor for an array of low cost microanalytical techniques for selective prompt and on-site recognition of duplicitous fluoride in semi-aqueous medium, J. Fluor. Chem. 249 (2021), 109858.
[35] D.A. Iovan, S. Jia, C.J. Chang, Inorganic chemistry approaches to activity-based sensing: from metal sensors to bioorthogonal metal chemistry, Inorg. Chem. 58 (2019) 13546–13560.
[36] Z. Chi, X. Ran, L.L. Shi, J. Lou, Y.M. Kuang, L.J. Guo, Molecular characteristics of a fluorescent chemosensor for the recognition of ferric ion based on photoresponsive azobenzene derivative, Spectrochim. Acta A. 171 (2017) 25–30.
[37] S.M. Hwang, M.S. Kim, M. Lee, M.H. Lim, C. Kim, Single fluorescent chemosensor for multiple targets: sequential detection of Al^{3+} and pyrophosphate and selective detection of F^- in near-perfect aqueous solution, New J. Chem. 41 (2017), 15590.
[38] S. Mabhai, M. Dolai, S.K. Dey, A. Dhara, S.M. Choudhury, B. Das, S. Dey, A. Jana, Rhodamine-azobenzene based single molecular probe for multiple ions sensing: Cu^{2+}, Al^{3+}, Cr^{3+} and its imaging in human lymphocyte cells, Spectrochim. Acta: Mol. Biomol. Spectrosc. 219 (2019) 319.
[39] A.J. Beneto, A. Siva, A phenanthroimidazole based effective colorimetric chemosensor for Copper(II) and Fluoride ions, Actuators B: Chem 247 (2017) 526–531.
[40] X.Y. Qu, Y.J. Bian, Y. Bai, Z. Shen, A visible BODIPY probe for "Naked-Eye" detection of pH value and intracellular Fe^{3+}, Chin. J. Inorg. Chem. 4 (2019) 649–657.
[41] Z.J. Lu, W.Z. Luo, X.N. Huang, H.X. Yu, Z.W. Li, G.C. Liu, L.W. Liu, X.X. Chen, Highly-stable cobalt metal organic framework with sheet-like structure for ultra-efficient water oxidation at high current density, J. Colloid Interface Sci. 611 (2022) 599–608.